Journal of Power Sources 196 (2011) 5573–5582

Contents lists available at ScienceDirect

Journal of Power Sources

journal homepage: www.elsevier.com/locate/jpowsour

Laser perforated fuel cell diffusion media. Part I: Related changes in performance and water content

M.P. Manahan[a], M.C. Hatzell[a], E.C. Kumbur[b], M.M. Mench[c,*]

[a] Fuel Cell Diagnostics and Dynamics Laboratory, Department of Mechanical and Nuclear Engineering, The Pennsylvania State University, University Park, PA 16802, USA
[b] Electrochemical Energy Systems Laboratory, Department of Mechanical Engineering and Mechanics, Drexel University, Philadelphia, PA 19104, USA
[c] Fuel Cell Diagnostics and Design Laboratory, Department of Mechanical, Aerospace, and Biomedical Engineering, University of Tennessee, Knoxville, TN 37996, USA

ARTICLE INFO

Article history:
Received 29 October 2010
Received in revised form 6 January 2011
Accepted 7 January 2011
Available online 14 January 2011

Keywords:
Diffusion media
Flooding
Neutron radiography
Polymer electrolyte fuel cell
Water management

ABSTRACT

In this study, cathode-side, bi-layered diffusion media (DM) samples with micro-porous layer were perforated with 300 μm laser-cut holes (covering 15% of the surface area in a homogenous pattern) using a ytterbium fiber laser to investigate the effect of structural changes on the gas and water transport. Under reduced humidity conditions (50% inlet relative humidity on the anode and cathode), the perforated DM were observed to increase the potential by an average of 6% for current densities ranging from 0.2 to 1.4 A cm^{-2}. However, the perforated DM showed reduced performance for current densities greater than 1.4 A cm^{-2} and at all currents under high-humidity conditions. Neutron radiography experiments were also performed to understand the changes in liquid water retention characteristics of DM due to the laser perforations. Significant water accumulation and water redistribution were observed in the perforated DM, which helps explain the observed performance behavior. The results indicate that the perforations act as water pooling and possible channeling locations, which significantly alter the water condensation, storage, and transport scheme within the fuel cell. These observations suggest that proper tailoring of fuel cell DM possesses significant potential to enable fuel cell operations with reduce liquid overhead and high performance.

1. Introduction

Water management is a deterministic factor in performance, stability, and durability of polymer electrolyte fuel cells (PEFCs). The major limiting aspect of the water management arises from multi-phase flow effects, which represent a major bottleneck, not only for efficient fuel cell operation, but also for operational stability and durability under prolonged operations. From a water management perspective, the porous diffusion medium (DM) is a critical component, as it functions to deliver reactant to, and products away from, the catalyst layer (CL) [1,2]. Since the transport in PEFCs involves both liquid and gas-phases, the fuel cell DM serves a critical role by enabling capillary transport of liquid away from the electrodes to avoid severe performance losses caused by flooding. Therefore, proper tailoring of fuel cell DM is critical to establish an optimal water management during PEFC operation.

The addition of a microporous layer (MPL) between the DM and CL has been shown to significantly improve cell performance (*e.g.*, [2–8]). In general, the MPL provides more smooth contact between DM and CL, reducing the electrical resistance between these layers, while serving as a protective layer to prevent the coarse DM fibers from puncturing through the CL and membrane. Some studies suggest that due to the small pore size, the MPL acts as a capillary barrier, directing the liquid water flow towards the anode side, helping membrane to maintain high hydration level [9,10]. However, recent experimental studies have been inconclusive on this topic [3–11]. For instance, recent studies revealed the existence of deep cracks and other surface defects on the MPL surface [4,12–14], which are argued to serve as preferential pathways for water removal from the cathode CL towards the MPL|DM interface [4,12]. A recent study by Owejan et al. [15] from GM also confirms this finding, suggesting that the primary role of MPL is to prevent condensed water from pooling at the CL rather than enhancing the capillary-driven transport towards anode side. The nature of the interface between the MPL and CL is also shown to be critically important to avoid interfacial delamination during freeze/thaw cycling [16,17].

Polytetrafluoroethylene (PTFE) in the CL, MPL, and DM has been shown to have a positive impact on fuel cell performance, and several optimization studies have been conducted (*e.g.*, [18–21]). The addition of PTFE was shown to create a mixture of hydrophilic and hydrophobic pores [2,21–24]. A majority of the efforts in this area were performed to analyze the effects of PTFE loading and developing methods to tailor and optimize the ratio of hydrophilic

* Corresponding author. Tel.: +1 865 974 6751; fax: +1 865 974 5274.
E-mail address: mmench@utk.edu (M.M. Mench).

0378-7753/$ – see front matter © 2011 Elsevier B.V. All rights reserved.
doi:10.1016/j.jpowsour.2011.01.014

and hydrophobic pores in the fuel cell DM [2,19,20,25–29]. From a transport perspective, hydrophilic pores are theoretically desirable to aid in wicking water away from reaction sites in order to minimize flooding and reduce liquid film generation; however, they can also act as water pooling locations that promote high DM saturation, which could foster flooding-related losses and durability concerns. Hydrophobic pores, on the other hand, have been shown to reduce the DM saturation [4,6,30]. Too many hydrophobic pores, however, can create a strong hydrophobic layer with high resistance to liquid water, promoting local water buildups at the MPL|CL interface, which promote poor electrical contact along the MPL|CL interface [19,31] and flooding related performance losses. Additionally, excessive PTFE content in the DM can impede evaporative removal of liquid water at shut down [32,33], causing retention of significant water inside the cell. Clearly, a proper mixture of hydrophilic and hydrophobic pores is necessary for optimal water transport with the fuel cell. It should be noted that beyond a simple balance between hydrophobic and hydrophilic pores, the connectivity and tortuosity are also critical to provide desirable transport of liquid and gas phases of product and reactant.

It is worthwhile to briefly discuss modes of liquid transport within DM. Especially at higher current, where heat generation and temperature gradients are more significant, phase-change-induced (PCI) flow is a key mode of water transport from the electrodes. In PCI flow, liquid water near the warmer CL evaporates, moves through the DM by diffusion, and then condenses in a colder location near or in the channel. PCI flow has been shown to be a significant mode of liquid water and heat transport, especially when bi-layered, PTFE-containing DM is present [34–36]. Another mode of transport within the porous DM is capillary flow [1,21–23,37]. Due to the small pore sizes, gravitational and viscous forces are relatively small compared to capillary forces. Depending on the operating conditions and materials used, capillary and PCI water transport mechanisms have varying degrees of dominance.

Another important factor affecting the water distribution inside the cell is the interfacial regions, such as that between MPL and CL. The impact of the MPL|CL interface morphology on water management of the fuel cell is not yet well-understood. Recent visualization studies have indicated that interfacial effects may be responsible for altering the saturation profile and water storage near the CL|MPL and MPL|DM interfaces [12–14,38,39]. To date, most fuel cell models assume the interfacial regions to be infinitely thin, having a perfect contact and homogenous in-plane properties [36,37]. As a result, they predict a sharp discontinuity at these interfaces due to the change in pore structure and hydrophobicity. However, recent experimental evidences obtained using X-ray tomography [38] and neutron imaging [39] have shown that this assumption can be in error. In a study by Hartnig et al. [38], significant water accumulation near the MPL surface is observed by using synchrotron X-ray. Similarly, Turhan et al. used neutron radiography and observed an inverted liquid-saturation jump distribution around these interfaces, which was attributed to water storage in MPL cracks and along the interface region [39]. Other studies [12–15] have also shown that the interfacial morphology of the CL and MPL (*i.e.*, surface cracking and irregularities) can lead to significant liquid water storage, altering the saturation values observed with neutron imaging.

Obtaining through-plane water distribution profiles has become increasingly important for understanding the water distribution in DM and improving the fidelity of models. More accurate measurement of through-plane liquid distribution profiles has recently become possible due to enhancements in high-resolution neutron radiography (NR) [40]. With the recent advancements in NR, many researchers have been able to better understand both liquid- and vapor-phase water transport in the DM. Hickner et al. [41] were able to investigate MEA hydration under different gas feed flow rates and current densities. They found that evaporative driven flow is critical for effective removal water from the cell. The results were further used to develop a model that rationalized observed water transport trends [42]. Other studies investigated passive methods for altering water distributions by customizing the channel wall hydrophobicity and manipulating PCI flow through controlled temperature gradients [39,43].

To date, there are contradictory hypotheses in the pertinent literature that portray the water transport mechanisms differently. Some suggest that capillary transport occurs in a tree-like structure, while an opposing concept proposes a fingering and channeling mechanism. In a study by Benziger et al. [30], it was proposed that the ideal DM should consist of a few large pores that transport and/or store liquid water (depending on hydrophobicity of the pores), and numerous small pores (*ca.* 40 μm) that are relatively free of liquid water and serve to transport the reactants. Gostick et al. [4] also suggested that introducing "large holes for water passage" may improve the effectiveness of the MPL. The general concept is to create a DM with ideal proportions of hydrophilic and hydrophobic pores in order to avoid excess water while preventing membrane dryout and oversaturation of the DM. Two groups [44–46] have published work studying the predictions of Refs. [4,30]. Studies have investigated the effect of introducing large-diameter holes into the DM, both along the channel path [44,46] and under a channel [46]. Both [45,46] have investigated cell stability changes with holes.

In this study, *in situ* measurements of unaltered and laser-perforated fuel cell DM were performed to examine the effects of tailored internal structure and modified pore characteristics of the DM on the performance and transport characteristics of PEFCs. Commercial DM samples coated with MPL were perforated with 300-μm laser-cut holes using a ytterbium fiber laser, and then subjected to extensive experimental evaluation. Similar studies in the literature [4,30] suggest that perforations or enhanced pore distribution could improve the effectiveness of the DM. In continuing along this trajectory, this study offers benchmark experimental data to help understand the dominance and role of PCI and capillary transport modes on the cell performance, and indicates that optimization of the DM structure is possible for reduced liquid overhead, but requires a detailed understanding of the complex water and heat transport phenomena inside the cell.

2. Experimental methods and setup

2.1. Laser perforation

A ytterbium fiber laser was used to introduce evenly-spaced through-holes, each with a diameter of 300 μm, to the cathode-side DM and MPL of a PEFC, covering approximately 15% of the total geometric surface area (see Fig. 1). Laser power level, pulse duration, and the distance between the last plano-convex lens and the DM surface were identified as the key parameters that affect the diameter and depth of the laser-cut holes [47]. Therefore, these key perforation parameters were optimized in order to achieve the desired perforation dimensions, and are listed in Table 1.

Laser perforation has the advantage of physically burning carbon/binder material away, instead of simply translating material to the surrounding areas, which may happen with micromachining techniques [44]. The use of a laser, however, causes a heat-affected zone (HAZ), which is the dark region surrounding the perforation shown in Fig. 1a [47]. The diameter of the HAZ is primarily dependent on the key laser perforation parameters previously described. The heat-affected zone was analyzed using an energy dispersive X-ray spectroscopy (EDS) and an environmental scanning electron microscope (ESEM) by Hizir [47]. The EDS showed only a domi-

Table 1
Parametric settings for laser perforations.

	Purpose	Power (Watt)	Duration (μs)	Lens to DM distance (mm)	D_{hole} (mm)	n_{hole}	X (mm)	Percent area with holes (%)
Cell size: 5 cm	Polarization testing at PSU	37	1500	27	0.300	1444	0.67	15
Cell size: 17.2 cm^2	Neutron imaging testing at NIST	37	1500	27	0.300	1920	0.97	7

D_{hole}, N_{hole} and X represent the diameter of the laser perforated holes, number of holes, and the distance between holes, respectively.

nant carbon peak in the heat-affected zone (Fig. 1c), indicating the absence of PTFE. The regions beyond the HAZ displayed carbon and fluorine peaks (Fig. 1d), indicating the presence of PTFE. The ESEM also showed a marked decrease in contact angle of water droplets in the heat-affected zone, indicating that the HAZ is more hydrophilic than the non-affected portion of the MPL surface. Therefore, the 300-μm perforations are expected to yield both a low capillary pressure zone (due to the comparatively large pore size of the perforation) and a hydrophilic region surrounding the perforation (due to the removal of PTFE), both of which are expected to promote water accumulation in, and near, these areas [47]. It is worthwhile to note that the laser perforation dimensions and pattern were chosen in order to mimic a pattern that could be easily implemented into industrial design.

2.2. In-situ polarization testing

In this study, SGL 10BB series DM samples coated with MPL (SIGRACET Gas Diffusion Layer™) and commercially available membrane electrode assemblies were used. The anode-side DM in each experiment remained unaltered, while the cathode DM used was varied as described. *In situ* testing was performed with a custom-designed, 5 cm^2 active area, double serpentine fuel cell using a Scriber Associates 850C Fuel Cell Test System. After careful assembly of the fuel cell components, each cell underwent a common break-in procedure involving 100% inlet relative humidity (RH) flow at the anode and cathode. The cell was cycled from open circuit voltage to 0.6 V and then 0.4 V at 1 min hold intervals. The cell was considered ready for experimentation when the current at 0.6 and 0.4 V no longer changes significantly with time. Regular experiments were conducted with over-humidified (120%/120% inlet RH anode/cathode) and low-humidity (50%/50% A/C) inlet reactant gases both at high (75 °C) and low (50 °C) temperatures. Nitrox (dry air) and heliox cathode gases, which contain N_2 and He as the inert cathode gas mixed with 21% O_2 in a dry state, respectively, were used. Flow rates were held constant at 139 and 332 sccm for the anode and the cathode at the atmospheric exit pressure, respectively.

Typically, at elevated temperatures, the rate of liquid water evaporation from the PEFC is higher, and gas-phase transport is more dominant. Conversely, lower temperature operation is expected to reduce evaporation rates, causing liquid water effects to be more important. The ratio of the limiting current of a cell with nitrox and heliox cathode gases can be compared to the ratio of the nitrogen and helium diffusivities in oxygen. This comparison can be used to quantify the relative dominance of molecular diffusion over other forms of diffusion, such as Knudsen diffusion. This approach is described in Refs. [48,49] and employed in this study to elucidate the gas- and liquid-phase transport phenomena associated with the introduction of laser perforations in the DM.

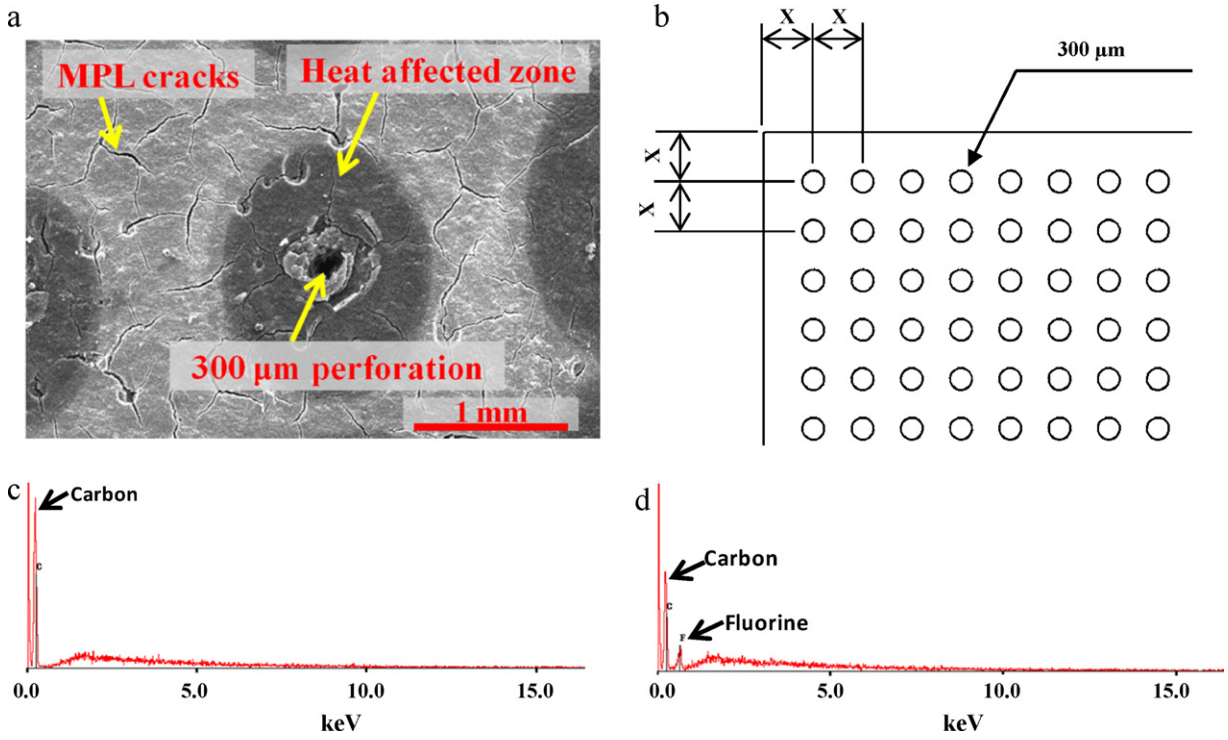

Fig. 1. (a) SEM image of the MPL surface with laser perforations. A heat-affected zone and 300-μm perforations are highlighted as key modifications due to the laser treatment, whereas the MPL cracks occur on both laser-treated and virgin samples; (b) Schematic of laser perforations, where x = 0.67 mm for polarization testing and 0.97 mm for NR testing; (c) An EDS spectrum of MPL surface within the heat affected zone. There is no fluorine peak, indicating the absence of PTFE; (d) An EDS spectrum of the virgin MPL surface, showing dominant carbon and fluorine peaks.

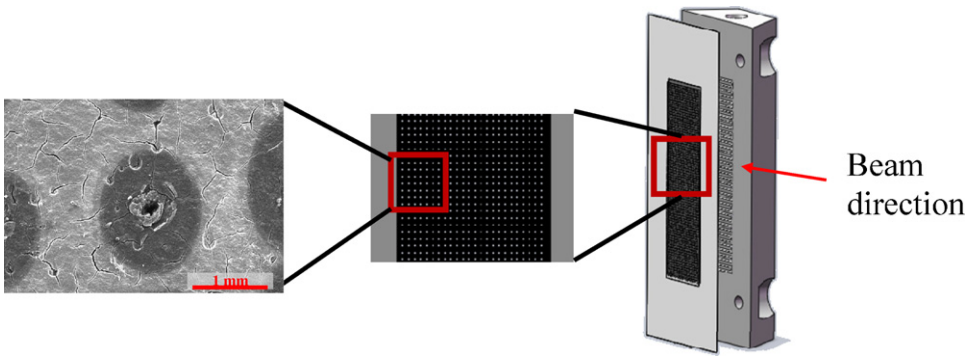

Fig. 2. Rendering of the neutron radiography test cell with expanded view of perforated DM schematic and SEM image.

To minimize the effects of hysteresis and ensure repeatability among tests, a pre-conditioning cycle, which includes 10 min of load cycling followed by 10 min of constant voltage, was conducted before each test. Furthermore, each cell was operated under galvanostatic mode for the duration of the polarization testing to ensure constant water generation in these tests. Each galvanostatic step was conducted for 3 min to achieve quasi-steady state conditions. To approach the limiting current under each condition, a 1-min potentiostatic step at 0.2 V was added to each polarization test. In some cases, especially those with perforated cathode-side DM, severe flooding has occurred at the final step, and the data could not be obtained. For comparison purposes, the cell voltage was compensated with the high frequency resistance (HFR) measured during testing in order to eliminate the losses due to membrane hydration differences. Finally, it should be noted that the error bars were added to the polarization data to indicate the level of repeatability from test to test. For all cases, 2–4 polarization sequences were conducted for the measurements being recorded. The upper and lower error bars given in the figures represent the highest and lowest average voltage response measured for any given current density, respectively.

2.3. Neutron radiography

In this study, neutron radiography (NR) testing was conducted to observe and quantify the changes in water management characteristics of virgin and perforated DM samples. Imaging was performed at the National Institute of Standards and Technology (NIST) in Gaithersburg, Maryland. The high-resolution imaging system at NIST has a resolution of *ca.* 13 μm, and the captured images have a nominal pixel pitch of 10 μm. The fuel cell was imaged in the through-plane direction, and a schematic of the cell and perforated DM is shown in Fig. 2.

In the NR experiments, the same cell components (SGL 10 BB series DM with MPL and commercially available membrane electrode assemblies) were used; however, the NR cell had an active area of 17.2 cm^2 with an in-plane to through-plane length ratio of *ca.* 0.3 for improved resolution. Perforated DM samples were prepared using the same technique described earlier. The samples used in NR testing had 300-μm diameter perforations with a center-to-center distance of 0.97 mm, which constituted *ca.* 7% of the geometric surface area of the DM samples. After appropriate break-in procedures, each cell (virgin and perforated DM) was operated at a constant current for 30 min at 65 °C under an inlet relative humidity of 100%/100% and 50%/50% (anode/cathode) at a stoichiometry of 2/2 hydrogen/nitrox (air). In high humidity cases, the current densities of 0.2 A cm^{-2} and 1.2 A cm^{-2} were selected, whereas the current densities of 0.2 A cm^{-2} and 1.7 A cm^{-2} were chosen for the low humidity case. During this 30-min interval, neutron images and performance data were collected under low and high humidity conditions to characterize the performance and quantify the water content differences between the virgin and perforated DM cases.

3. Results and discussion

3.1. Effect of perforations on performance and water accumulation

The following sections describe the results of low and high humidity testing of both perforated and unaltered DM cases. The polarization testing was conducted at the Pennsylvania State University, and the neutron imaging tests were performed at NIST (Gaithersburg, MD). A fuel cell fixture with DM that has perforations corresponding to 15% geometric area of the DM was used for the polarization testing, while a fuel cell with DM that has perforations corresponding to 7% geometric area of the DM was utilized for the neutron imaging testing. It was observed that the measured performance trends of the 15% and 7% perforated DM show very similar behavior, indicating that the similar physical phenomena exist in the 15% and 7% perforated DM cases.

3.1.1. Low humidity testing

3.1.1.1. Polarization testing at low humidity conditions. In these tests, cell fixtures with a perforated cathode-side DM and with a virgin (unaltered) cathode-side DM were exposed to low humidity conditions (50% relative humidity) with nitrox (21% O_2 and 79% N_2) as the inlet cathode gas. Fig. 3 shows the IR-compensated polarization data of these two cases obtained at low humidity condition.

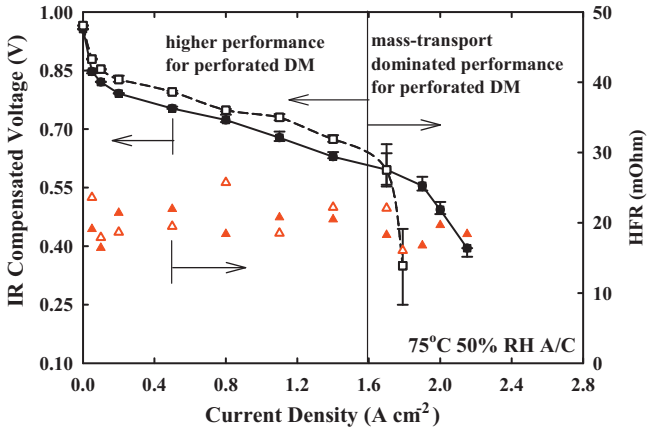

Fig. 3. Performance data for 75 °C, 50% relative humidity, nitrox conditions with virgin DM (–■–), 15% 300-μm perforated cathode-side DM (- -□- -), and corresponding HFR values for the virgin (▲) and perforated (△) cases. Perforated DM shows on average 38 mV higher potential in current densities <1.4 A cm^{-2} but fail to achieve steady state at current densities greater than 1.4 A cm^{-2}.

As shown in Fig. 3, the perforated DM case is observed to exhibit an average of 38 mV (6%) higher potential for the current densities ranging from 0.1 to 1.4 A cm^{-2}. Above 1.4 A cm^{-2}, however, the losses are observed to rapidly increase, and the cell could not sustain quasi-steady performance beyond 1.6 A cm^{-2}. A maximum current density of 1.79 A cm^{-2} was recorded at 0.2 V for the perforated DM case, whereas the cell with unaltered DM was observed to draw a 20% higher maximum current density of 2.15 A cm^{-2} at 0.2 V.

While the perforated DM shows an increase in performance in the *lower* current regions, the significant performance drop in the *higher* current regions (*i.e.*, greater than 1.4 A cm^{-2}) indicates the existence of significantly increased mass transport losses due to the perforations in the DM (Fig. 3). Beyond 1.6 A cm^{-2}, the performance of the cell with perforated DM is highly unstable. While comparable error bars between the two cells are seen at 1.6 A cm^{-2}, the virgin cell was observed to quickly recover the mass transport losses and regain stability as it effectively removes liquid water build-ups from reaction sites. The observed difference in performance of these two cases at low humidity conditions can be attributed to the altered mass transport caused by the perforations. At low humidity, the redirection of water into the perforated regions appears to enhance oxygen transport to the catalyst, while at higher current, flooding occurs as a result of the additional perforations.

In terms of HFR measurements, the two cases—perforated and virgin DM—interestingly did not show any particular correlation at low humidity conditions; that is, neither case showed consistently higher or lower resistance values over each other within the entire current density range. This indicates that the increase in electron path around the perforations does not cause a substantial increase in the overall measured cell resistance, and the bulk ohmic resistance in the membrane is not significantly affected by the presence/absence of DM perforations for the tested conditions. It should be noted that the HFR will mostly not record changes in the CL ionic conductivity, however, so dryout of the CL is not indicated by the HFR response. The similar cell resistances observed for these two cases can be explained by the relatively high in-plane electronic conductivity of the DM and CL materials [50], which appears to compensate the additional path of resistance introduced by perforations.

In terms of membrane resistance, similar values can be explained through analyzing the changes in the water transport patterns inside the cell due to the addition of perforations. In general, the MPL serves to provide smooth contact between the DM and the CL, and can act as a capillary barrier to avoid excess water accumulation to the pores of the DM [8,10,37]. Since the perforations effectively eliminate a certain portion of this barrier, one can argue that water would be less readily retained in the perforated case, leading to membrane dehydration, especially under low humidity conditions. Though notable membrane dehydration was not observed in this study, it may indeed occur if even lower inlet humidity conditions are used. However, the hydrophilic and low-capillary pressure nature of the perforated regions may enable significant amount of water storage, especially at high current conditions. Once fully saturated, the water stored in the perforated regions can feed the CL and membrane, enabling it to retain similar hydration level as compared to the unaltered DM case, which would yield comparable ohmic resistance values, as observed in the HFR testing (Fig. 3).

3.1.1.2. Neutron radiography testing – virgin vs. perforated DM. To further analyze the potential impact of perforations on the cell performance, neutron imaging tests were performed under *low humidity* conditions. Interestingly, for low current densities, neutron images indicate negligible differences in total water amount between the virgin and perforated DM, as shown in Fig. 4a. While the total water amount in the cell is approximately the same, the perforations redistribute the water (discussed later), which may be the cause for the increased performance. At lower current densities, the perforations may (a) act as water pooling locations, thus opening previously filled pores for gas transport and/or (b) serve as large-diameter gas conduits, depending on the amount of liquid water present. Both options could increase the gas access to the CL, which would increase the species concentration at the electrode, hence reducing the polarization and increasing performance. At higher current (Fig. 4b), however, the perforated DM is observed to have significantly higher liquid water mass in all locations, most likely due to the increased water pooling in the perforations sites. The measured water mass values at high current densities also show distinct water distribution trends, which are plotted in Figs. 4 and 5. These results were obtained by extracting water thickness measurements from pixels in the membrane/DM region of the cell in both the in-plane and through-plane direction of the fuel cell.

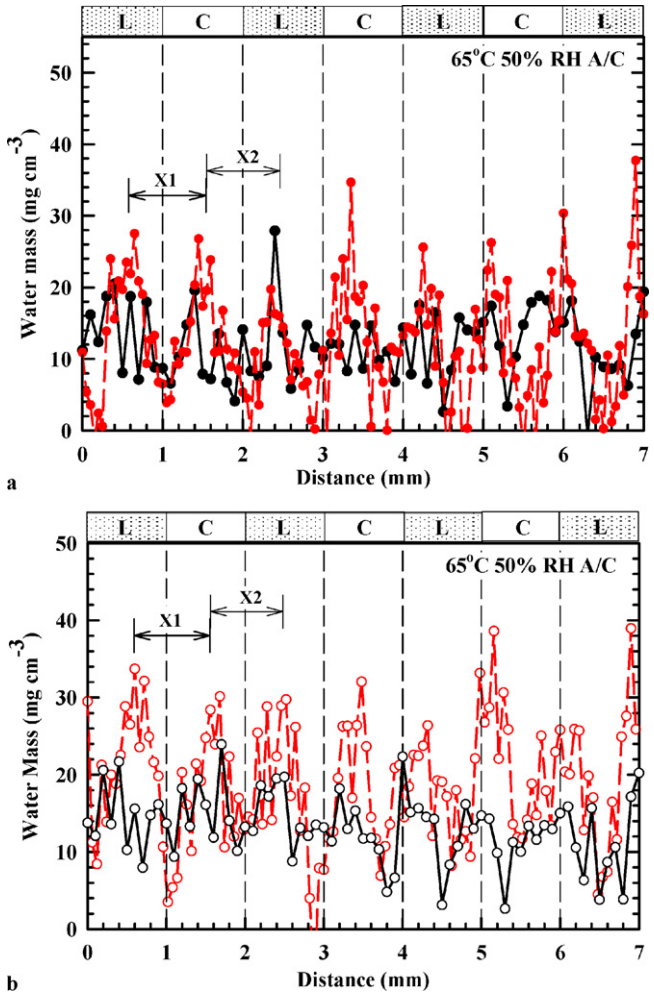

Fig. 4. Neutron data for water mass per volume distributions in the in-plane direction at low inlet relative humidity condition. L represents land, and C represents channel. (a) Water distributions for virgin DM (–●–) and perforated DM (- -●- -) under low current density (0.2 A cm^{-2}) testing operation and (b) water distributions for virgin DM (–○–) and perforated DM (- -○- -) under high current density (1.7 A cm^{-2}) testing operation. A reduced number of data points are shown to improve clarity.

In Fig. 4, $x = 0$ mm corresponds to a row of pixels normal to a centrally-located land|channel interface, and $x = 7$ mm corresponds to the length of four lands and three channels (each 1 mm wide).

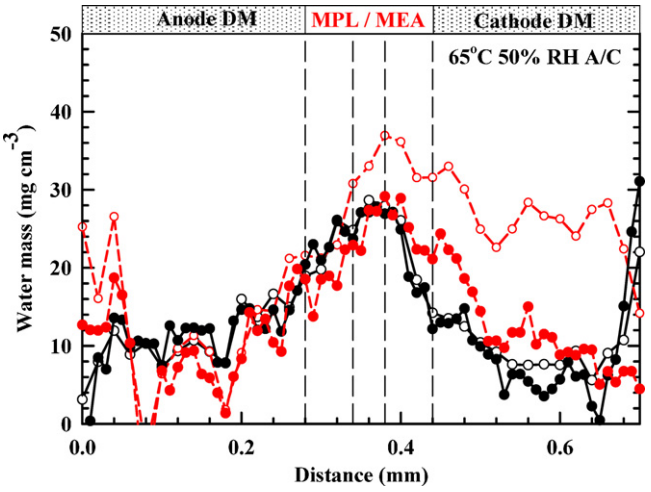

Fig. 5. Neutron data for water mass per volume distributions in the through-plane direction at low inlet relative humidity condition. Virgin case at high current (–○–), virgin case at low current (–●–), perforated DM case at high current (- -○- -), perforated DM case at low current (- -● - -). A reduced number of data points are shown to improve clarity.

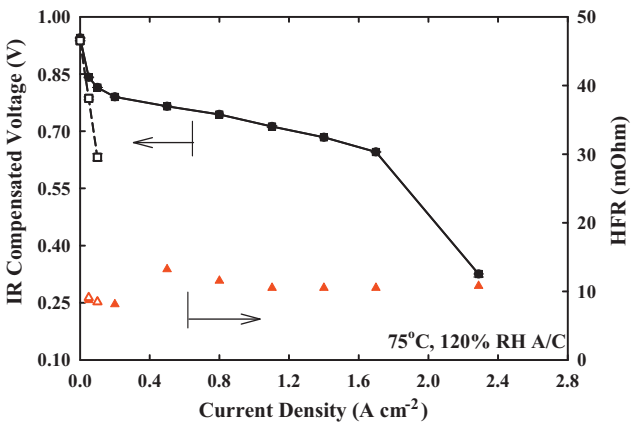

Fig. 6. Performance data of 75 °C, 120% relative humidity, nitrox conditions for virgin DM case (–■–), 15% 300-μm perforated cathode DM case (- -□- -), and corresponding HFR values for the virgin (▲) and perforated (△) cases. The DM perforations cause drastic performance losses (55 and 183 mV at 0.05 and 0.1 A cm^{-2}, respectively), indicating poor water management in high humidity conditions.

The secondary *x*-axis is included to clarify the locations from which water mass values were extracted. In both low and high current density conditions, the periodic peaks in the *perforated DM* are observed at locations corresponding to $x = 0.56$, 1.53, 2.48, 3.37, 4.22, 5.16, 6.07, 6.89 mm (Fig. 4). These periodic peaks, which are not observed in the virgin DM case, indicate the possible pooling locations induced by the perforations, which had a center-to-center distance of *ca.* 0.97 mm. In a recent study by Gerteisen and Sadeler [45], it has been suggested that perforations may create paths of least resistance for water to flow through the DM towards the channels. These preferential pathways would correspondingly impede the capillary fingering transport mode that typically takes place in the hydrophilic pore network of DM [51]. The present neutron imaging results—namely the periodic peaks observed at perforation locations—experimentally verify this hypothesis. Furthermore, the local minima on either side of the peaks in the perforated DM show *lower* water mass values than the ones at the corresponding location in the virgin DM case, indicating that the water has translocated from the bulk DM into the hydrophilic perforation regions. Therefore, it can be hypothesized that under low-humidity operating conditions, the perforated DM exhibits the potential benefit of dictating the preferred path of liquid water in the water management process. To the best of the authors' knowledge, this is the first reported experimental validation of this phenomenon. As can be ascertained, then, perforations may be used as a passive method to dictate water migration paths in the DM.

When the low humidity/high current data in Fig. 4b are integrated across the *x*-axis, the results show that the perforated DM contains 46% more water mass than the virgin DM at 1.7 A cm^{-2}. From Fig. 5, it is clear that this additional 46% water mass is a result of the accumulated water in the perforated regions at the cathode. The water accumulation into perforated regions can be explained by analyzing the water transport modes inside the cell. It is hypothesized that the prime modes of liquid water removal can be altered by the presence of the perforations. For instance, phase-change-induced (PCI) flow is considered as a prominent mode of water transport within the PEFCs. It was shown [34] that the PCI flows tend to increase with hydrophobic content in the DM regardless of the temperature gradient, since PCI flow is dependent on the presence of a vapor zone. Since the laser pyrolyzes the PTFE coatings at the vicinity of the perforated regions (*i.e.*, making these regions more hydrophilic), it is very likely that the water removal by PCI flow would become less favorable in the perforated DM. In addition, it is very likely that the capillary flow can be inhibited by the perforations, such that introducing large perforations (300-μm, as in this study) significantly decreases the capillary pressure due to the increased pore size, impeding the removal of liquid water via capillary-driven transport within the cell. As a result, water accumulation is more likely to dominate the performance of the perforated DM cell at higher current operations.

3.1.1.3. Neutron radiography testing – high vs. low current at low humidity operations. In addition to the side-by-side comparison of the virgin and perforated DM, it is noteworthy to compare how each diffusion media variety responds to the increase in water production from low to high current. At *low current* (Figs. 4a and 5), the perforated DM only contains 2% more water mass than the virgin DM. Since relatively little water is entering the cell via the partially-humidified gases, and relatively little water is produced at the CL at low current, the difference between the amount of water stored in the cell for the virgin and perforated case is expected to be minimal. In other words, the amount of liquid water in the DM is not significant at these conditions, thus the water management differences between virgin and perforated DM are otherwise insignificant.

At *high current densities*, the perforated DM contains 33% more water at high current than at low current, whereas the virgin DM only shows a 4% increase from low to high current. It is reported that at higher current, the PCI flow plays a critical role in removal of liquid water from the cell [42]. Thus, since the PCI flow dominance is severely reduced with the perforated DM (due to the loss of hydrophobic binder and the introduction of artificial flow conduits), it is very likely that there would be higher water mass accumulation in the perforated DM case as compared to the virgin DM under the high current densities. Fig. 5 clearly supports this argument, showing higher water accumulation in the perforated DM than the virgin DM case.

3.1.2. High humidity testing

3.1.2.1. Polarization testing at high humidity conditions. Fig. 6 shows the *high humidity* condition (120% inlet relative humidity anode and cathode) performance data for the same setup previously described. As seen in Fig. 6, the perforated DM case exhibits extremely poor performance under high humidity condition, showing a 183 mV lower potential than the virgin DM at a current density of 0.1 A cm^{-2}. Furthermore, it was not possible to reach stable operations higher than 0.1 A cm^{-2} for the perforated DM. The virgin

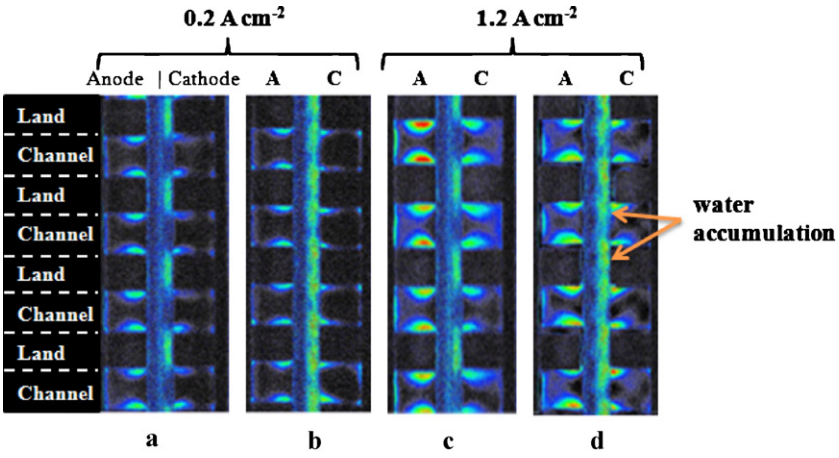

Fig. 7. Neutron images from high humidity (100% inlet relative humidity anode and cathode) testing, showing: (a) high current (1.2 A cm^{-2}) for virgin DM case; (b) high current for perforated DM case; (c) low current (0.2 A cm^{-2}) for virgin DM case; and (d) low current for perforated DM case. Note: a visual effect was removed from the black area that does not affect quantitative data. In each image, the right-hand-side represents the cathode.

DM, however, was capable of achieving limiting current densities *ca.* 2.3 A cm^{-2}. This drastic performance difference can be directly attributed to the water management differences between the cells. The over humidification of the cell facilitates the condensation of water generated during operation. The increase in condensed liquid water enhances the water accumulation and promotes the formation of liquid water buildup, which prevents reactants from accessing the reaction sites. As a result, the mass transport losses dominate the polarization of the cell, even at low current. While the cell with perforated DM cannot handle the excess liquid water, the PCI flow and capillary-driven transport appear to properly manage the water distribution within the cell for the virgin DM case.

Before presenting neutron imaging data on these test conditions, it is beneficial to note the reasons of poor performance and instability of the perforated DM at high-current and/or high-humidity operation, as shown in Figs. 3 and 6. The decreased performance observed at high current density is in conflict with the data presented by Gerteisen et al. [44], where it was shown that the implementation of DM perforations *increased* the limiting current density by 8–22%.

Four key observations should be made to explain this difference. First, the polarization testing reported in [44] was performed comparatively at low relative humidity conditions, thus their results are similar to the observations at the low humidity conditions presented herein. Secondly, the diameter of the perforations used by [44] was approximately 100 μm, which is 1/3 of the size of the perforations (300-μm diameter) presented in the current study. The relatively smaller diameter of the holes in [44] significantly enhances the capillary-driven water transport, causing liquid water to be more readily wicked away from the perforated regions and CL. Furthermore, as [46] notes, larger diameter pores, especially those under the channels, may lead to increased film coverage in the channels, leading to blockage of the reactant gases. Due to the high humidity scenario presented here, thin film coverage is likely. Further testing should be performed to determine the relation between the size/geometry of perforations and overall water distribution inside the cell, as this is obviously a key controlling parameter for intelligent selection of perforation geometry and layout. Another possible reason for this observed discrepancy may stem from the fact that the perforations reported in [44] were performed only adjacent to the channel locations, which corresponds to <1% of the total area. However, in the present study, the perforations were uniformly disturbed across 7 or 15% of the geometric area of the DM, covering both land and channel locations. Increased coverage area of perforation might have caused the observed performance difference between these two studies. Finally, in [44], a scan rate of 10 mV s^{-1} was used to obtain polarization data, which yielded 8–22% increase in limiting current of the cell for the perforated case. This is distinctly different from the test procedure that was followed in the present study, where the quasi-steady state measurements of 3-min dwell intervals were performed to obtain performance data for the tested cases. It is anticipated that the quasi-steady state measurements would allow for more accurate quantification of the impact of water accumulation inside the cell on the cell performance, whereas the use of a rapid voltage scan rate may display mostly the transient behavior of the perforations. The salient aspect of this comparison is to emphasize the evidence that an optimized perforated structure can yield desired performance metrics both under low *and* high humidity conditions, but this can only be achieved by careful consideration of various system parameters, which encourages further investigation.

3.1.2.2. Neutron radiography testing – virgin vs. perforated DM. Fig. 7 displays neutron images obtained under *high humidity* (100% inlet relative humidity) conditions. Images in Fig. 7a and c show neutron data for the virgin DM at high and low current, respectively, whereas images in Fig. 7b and d are the perforated DM case at high and low current operation, respectively. Qualitatively, the perforated DM images show significantly more water accumulation than the virgin DM case. The most notable observation is the significant water accumulation (both under lands and channels) for the perforated DM case, which clearly indicates that the perforations enhance the liquid water storage in the cell regardless of humidity condition. Such a feature across the entire active area may be beneficial for low relative humidity operation (for membrane hydration), but not for high relative humidity operation. Other studies [44,45] have shown that the perforated DM improves cell performance at high current operations, indicating that there is a significant potential to optimize both low and high humidity operation by altering the perforation size, location and cell geometry.

Figs. 8 and 9 show the quantitative values of in-plane and through-plane water content of these cases obtained from the neutron images shown in Fig. 7, respectively. For all the tested conditions, the total water mass per volume of the DM was observed to be higher in the perforated case than the virgin DM. At low current operation (Fig. 8a), the total water amount in the perforated DM was measured to be 38% higher than the virgin DM, and similarly, the perforated DM was observed to contain 30% more water mass under high current/high humidity conditions (Fig. 8b).

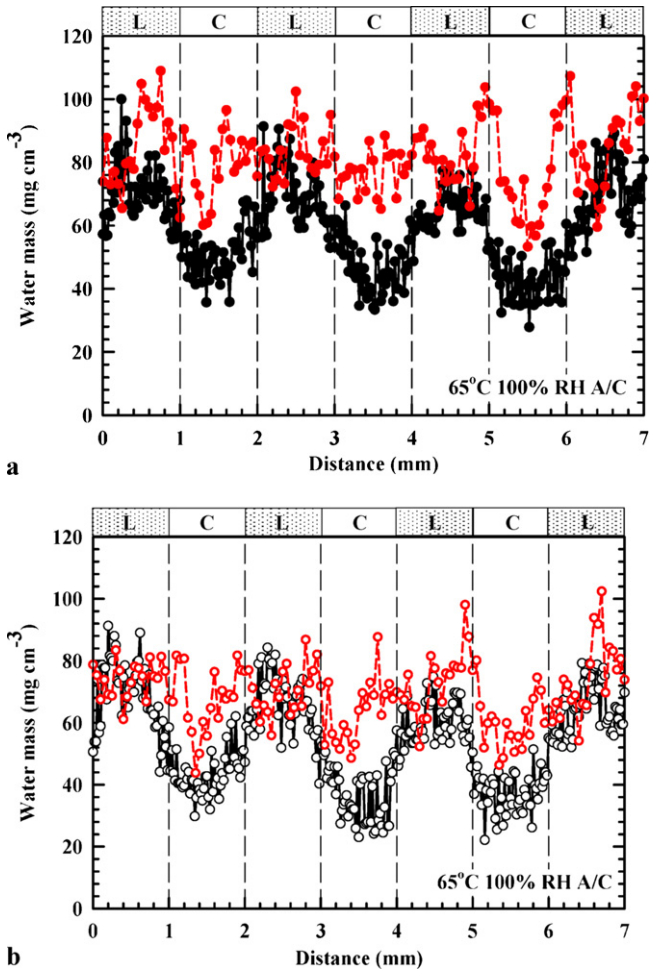

Fig. 8. Neutron data for water mass per volume distributions in the in-plane direction at high inlet relative humidity condition. L represents land, and C represents channel. (a) Water distributions for virgin DM (–●–) and perforated DM (- -● - -) under low current density (0.2 A cm^{-2}) testing operation and (b) water distributions for virgin DM (–○–) and perforated DM (- -○ - -) under high current density (1.7 A cm^{-2}) testing operation. A reduced number of data points are shown to improve clarity.

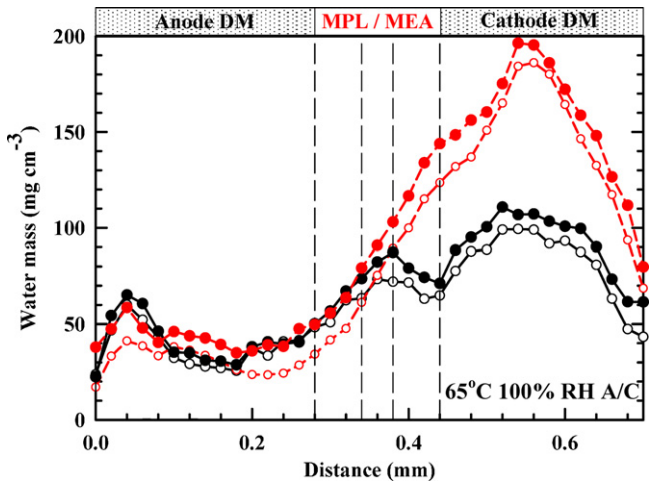

Fig. 9. Neutron data for water mass per volume distributions in the through-plane direction at high inlet relative humidity condition. Virgin case at high current (–○–), virgin case at low current (–●–), perforated DM case at high current (- -○ - -), perforated DM case at low current (- -● - -). A reduced number of data points are shown to improve clarity.

As previously discussed, the EDS and ESEM analysis showed that the area surrounding the laser perforations was more hydrophilic due to the removal of the PTFE during laser-perforation process. It is very likely that these highly hydrophilic regions may facilitate the condensation of water vapor and liquid storage in these regions, especially at high relative humidity condition. Previous studies [52] have shown that vapor phase diffusion preferably takes place through the hydrophobic DM, causing the vapor flux to condense under the landings and along the channel walls. With the introduction of the large hydrophilic perforations, the condensation locations can be altered in a way that excessive water accumulation would be encouraged, especially towards the perforated regions inside the DM, causing significant performance drop during operation.

Fig. 9 shows the water mass per volume distribution (in the through-plane direction) of unaltered and perforated DM cases at high humidity condition. As seen in Fig. 9, the perforated-DM water profiles steadily increase through the cathode-side MPL region and through half of the macro-DM substrate. However, significantly lower water content is observed for the virgin case. A similar trend is also seen in Fig. 5, where a sharp drop in the MPL region water mass is observed for virgin DM case. Perforations in the DM structure may also impede the function of the MPL to restrict water backflow from the DM into the CL, which could result in significant water coverage at the CL and consequently severe performance drop, as observed in Fig. 6. The water mass peaks observed mid-way through the macro-DM substrate in Fig. 9 support this argument, showing the existence of significant water diffusion gradient for the perforated DM case.

3.1.2.3. Neutron radiography testing – high vs. low current at high humidity condition. Neutron imaging was also performed for perforated and virgin DM cases under high humidity conditions at different current densities. The perforated DM was observed to contain 14% less water at high current (Fig. 8b) than at low current (Fig. 8a). The same trend was also observed for the virgin DM case, where the virgin DM is observed to retain 9% less water at high current. It should be noted that this behavior was the *opposite* of what was observed at low humidity operation. To explain this phenomenon observed at high humidity condition, several factors need to be carefully analyzed. First, PCI flow may be present at low *and* high current, but is certainly more dominant at higher current densities due to the steeper temperature gradients [34]. Therefore, the magnitude of water removal by PCI flow at elevated current would be higher, causing the low current operation (with lower temperature gradients) to retain higher water mass, as observed. Secondly, with the increased inlet relative humidity, it is expected that there will be an increase in water vapor condensation throughout the cell. The increased water saturation will further enhance the capillary-driven water transport, especially in the connected water pathways of DM [51,53]. Along with the high shear forces in the gas channel (due to high current operation), the increased PCI flow and enhanced capillary-driven water removal can explain the lower water content observed at high current density operation.

3.2. Effects of perforations on reactant transport

The effect of the perforations on the diffusivity of the reactants was studied by variation of the inlet cathode streams. As described in a previous work by our group [48], the ratio of the limiting currents measured using two different cathode-stream gases, namely nitrox and heliox (21% O_2 and 79% He), can be compared to the ratio of the molecular diffusivity values of oxygen in nitrogen and helium [49]. Comparing these ratios can yield information regarding the importance/dominance of Fickian diffusion as compared to other

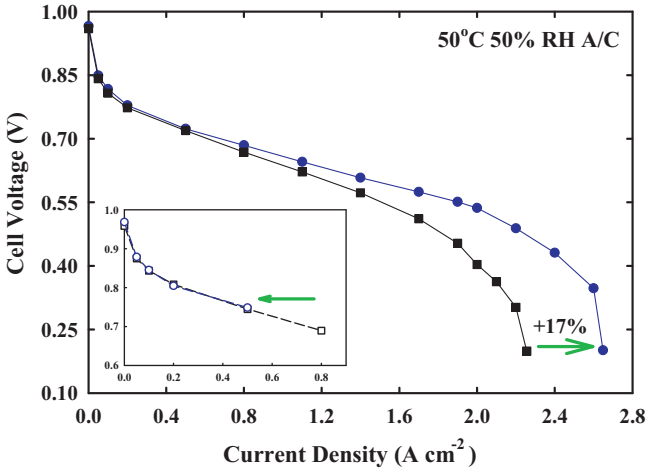

Fig. 10. Limiting current density comparison of 50 °C, 50% relative humidity conditions for the virgin DM case (main plot) and perforated DM case (inset). Virgin DM shows increases in the limiting current density when changing the cathode-gases from nitrox (–■–) to heliox (–●–), as expected and previously observed [48]. On the contrary, the perforated DM (inset) shows a decrease when switching from nitrox (--□--) to heliox (--○--), indicating the dominance of water accumulation in the DM and CL.

forms of diffusion. Detailed information regarding this analysis can be found in [48].

Fig. 10 highlights the 17% increase in limiting current observed with virgin DM when the inert gas is changed from nitrogen to helium at cathode. This was also observed in [48]. The inset in Fig. 10, showing the same analysis for the perforated DM, produced a deviation from the expected result. In theory, it was anticipated to observe a similar trend as in the virgin case, possibly with higher Fickian diffusion due to the large-diameter perforations. However, the experiments yielded an unexpectedly *higher* limiting current density (0.8 A cm^{-2}) for the nitrox than for the heliox case (0.5 A cm^{-2}). It is conjectured that this was due to increased water content in the perforated DM, causing the reactant flow rates to become a key factor in convective removal of accumulated water. In these tests, the heliox flow rate was set to be 25% lower than the nitrox flow rate due to the adjustments required for the mass flow controllers to maintain the equivalent oxygen concentration. This resulted in reduced water removal by convection and shear/drag effects in the flow channel. It is also expected that liquid water accumulation occurs more readily in the lower temperature operation, leading to flooding even at lower current densities than those observed at high temperature operations. Therefore, it can be hypothesized that the water removed in the perforated DM experimented is more sensitive to the role that flow rates play in water removal compared to the virgin DM.

4. Conclusions

This paper presents investigations of the *in situ* performance characteristics of virgin (unaltered) and laser-perforated DM (cathode-side only) by employing polarization testing and neutron radiography. DM samples were perforated with 300-μm laser-cut holes using a ytterbium fiber laser and compared to a virgin DM to investigate the effect of structural modifications on the water and gas transport characteristics of a PEFC. The perforated DM under low-humidity conditions (50% inlet relative humidity) showed on average a 6% voltage increase over the virgin DM for current densities ranging from 0.2 to 1.4 A cm^{-2}. However, the cell assembled with perforated DM was observed to experience severe performance drop under low-humidity operation at high current (greater than 1.4 A cm^{-2}), and at all currents under high-humidity operation (120% inlet relative humidity). The neutron radiography results showed that the perforations act as water pooling locations, collecting and/or channeling water from the surrounding DM and CL. It was observed that large laser perforations alter the impact of phase-change-induced flow in removal of excess water from the DM. Furthermore, it is hypothesized that the removal of the PTFE binder due to the laser processing is crucial to the performance stability as the loss of hydrophobicity can further promote liquid water accumulation to the perforation regions, yielding significant water buildups that can cause local flooding. The results of this study, along with the other efforts in the literature [44,45], suggest that proper tailoring of fuel cell DM (*i.e.*, adjusting the perforation size, geometry and location) possesses significant potential to enable PEFC operations with reduced liquid overhead and higher performance under a wide range of operating conditions. Studies are underway to further optimize and analyze the effects of the perforations geometry on the PEFC performance.

Acknowledgements

The authors would like to thank Prof. A. Turhan at the University of Tennessee Knoxville, and Drs. D.S. Hussey and D. Jacobson at NIST for their assistance with the neutron testing and data analysis, and Toyota Motor Company for partial support. Prof. M.M. Mench wishes to acknowledge the support for the work from NSF CAREER Award CBET #0644811, and Mr. M. Manahan would like to thank the NSF Graduate Research Fellowship Program for partial financial support on this project. The authors would also like to thank Mr. F.E. Hizir for performing perforations and SEM/EDS analysis, valuable discussions on the selection of perforation geometry, and analysis of a portion of the results.

References

[1] A. Bazylak, D. Sinton, N. Djilali, J. Power Sources 176 (2008) 240–246.
[2] M. Mathias, J. Roth, J. Fleming, W. Lehnert, in: W. Vielstich, A. Lamm, H.A. Gasteiger (Eds.), Handbook of Fuel Cells: Fundamentals, Technology and Application, John Wiley & Sons, 2003 (Chapter 46).
[3] H.K. Atiyeh, K. Karan, B. Peppley, A. Phoenix, E. Halliop, J. Pharoah, J. Power Sources 170 (2007) 111–121.
[4] J.T. Gostick, M.A. Ioannidis, M.W. Fowler, M.D. Pritzker, Electrochem. Commun. 11 (2009) 576–579.
[5] S. Park, J.-W. Lee, B.N. Popov, J. Power Sources 163 (2006) 357–363.
[6] J.H. Nam, M. Kaviany, Int. J. Heat Mass Transfer 46 (2003) 4595–4611.
[7] M. Mathias, J. Roth, J. Fleming, W. Lehnert, in: W. Vielstich, A. Lamm, H.A. Gasteiger (Eds.), Handbook of Fuel Cells: Fundamentals, Technology and Applications, John Wiley & Sons, New York, 2003 (Chapter 42).
[8] R.P. Ramasamy, E.C. Kumbur, M.M. Mench, W. Liu, D. Moore, M. Murthy, Int. J. Hydrogen Energy 33 (2008) 3351–3367.
[9] H. Meng, Int. J. Hydrogen Energy 34 (2009) 5488–5497.
[10] A.Z. Weber, J. Newman, J. Electrochem. Soc. 152 (2005) A677–A688.
[11] S. Ge, C.-Y. Wang, J. Electrochem. Soc. 154 (2007) B998–B1005.
[12] F.E. Hizir, S.O. Ural, E.C. Kumbur, M.M. Mench, J. Power Sources 195 (2010) 3463–3471.
[13] T. Swamy, E.C. Kumbur, M.M. Mench, J. Electrochem. Soc. 157 (2009) B77–B85.
[14] H. Bajpai, M. Khandelwal, E.C. Kumbur, M.M. Mench, J. Power Sources 195 (2010) 4196–4205.
[15] J.P. Owejan, J.E. Owejan, W. Gu, T.A. Trabold, T.W. Tighe, M.F. Mathias, J. Electrochem. Soc. 157 (2010) B1456–B1464.
[16] S. Kim, M.M. Mench, J. Power Sources 174 (2007) 206–220.
[17] S. Kim, B.K. Ahn, M.M. Mench, J. Power Sources 179 (2008) 140–146.
[18] W. Dai, H. Wang, X.-Z. Yuan, J. Martin, J. Shen, M. Pan, Z. Luo, J. Power Sources 188 (2009) 122–126.
[19] S. Park, B.N. Popov, Fuel 88 (2009) 2068–2073.
[20] S. Park, J.-W. Lee, B.N. Popov, J. Power Sources 177 (2008) 457–463.
[21] E.C. Kumbur, K.V. Sharp, M.M. Mench, J. Electrochem. Soc. 154 (2007) B1295–B1304.
[22] E.C. Kumbur, K.V. Sharp, M.M. Mench, J. Electrochem. Soc. 154 (2007) B1305–B1314.
[23] E.C. Kumbur, K.V. Sharp, M.M. Mench, J. Electrochem. Soc. 154 (2007) B1315–B1324.
[24] J.T. Gostick, M.W. Fowler, M.A. Ioannidis, M.D. Pritzker, Y.M. Volfkovich, A. Sakars, J. Power Sources 156 (2006) 375–387.
[25] Z. Qi, A. Kaufman, J. Power Sources 109 (2002) 38–46.

[26] L. Giorgi, E. Antolini, A. Pozio, E. Passalacqua, Electrochim. Acta 43 (1998) 3675–3680.
[27] F. Lufrano, E. Passalacqua, G. Squadrito, A. Patti, L. Giorgi, J. Appl. Electrochem. 29 (1999) 445–448.
[28] G. Velayutham, J. Kaushik, N. Rajalakshmi, K.S. Dhathathreyan, Fuel Cells 7 (2007) 314–318.
[29] R.R. Fredley, Porous support layer for an electrochemical cell, US Patent # 5,998,058 (1999).
[30] J. Benziger, J. Nehlsen, D. Blackwell, T. Brennan, J. Itescu, J. Membr. Sci. 261 (2005) 98–106.
[31] G.-G. Park, Y.-J. Sohn, T.-H. Yang, Y.-G. Yoon, W.-Y. Lee, C.-S. Kim, J. Power Sources 131 (2004) 182–187.
[32] K.T. Cho, M.M. Mench, J. Power Sources 195 (2010) 3858–3869.
[33] K.T. Cho, M.M. Mench, J. Power Sources 195 (2010) 6748–6757.
[34] S. Kim, M.M. Mench, J. Electrochem. Soc. 156 (2009) B353–B362.
[35] A.Z. Weber, J. Newman, J. Electrochem. Soc. 153 (2006) A2205–A2214.
[36] Y. Wang, C.-Y. Wang, J. Electrochem. Soc. 153 (2006) A1193–A1200.
[37] U. Pasaogullari, C.-Y. Wang, Electrochim. Acta 49 (2004) 4359–4369.
[38] C. Hartnig, I. Manke, R. Kuhn, N. Kardjilov, J. Banhart, W. Lehnert, Appl. Phys. Lett. 92 (2008) 134103–134106.
[39] A. Turhan, S. Kim, M. Hatzell, M.M. Mench, Electrochim. Acta 55 (2010) 2734–2745.
[40] D.S. Hussey, D.L. Jacobson, M. Arif, J.P. Owejan, J.J. Gagliardo, T.A. Trabold, J. Power Sources 172 (2007) 225–228.
[41] M.A. Hickner, N.P. Siegel, K.S. Chen, D.S. Hussey, D.L. Jacobson, M. Arif, J. Electrochem. Soc. 155 (2008) B427–B434.
[42] A.Z. Weber, M.A. Hickner, Electrochim. Acta 53 (2008) 7668–7674.
[43] A. Turhan, S. Kim, M. Hatzell, M.M. Mench, Electrochim. Acta 55 (2010) 2734–2745.
[44] D. Gerteisen, T. Heilmann, C. Ziegler, J. Power Sources 177 (2008) 348–354.
[45] D. Gerteisen, C. Sadeler, J. Power Sources 195 (2010) 5252–5257.
[46] E. Kimball, J. Benziger, Y. Kevrekidis, Fuel Cells 10 (2010) 530–544.
[47] F.E. Hizir, Characterization and tailoring of the microporous layer|catalyst layer interfacial structure in polymer electrolyte membrane fuel cells, Master of Science in Mechanical Engineering, The Pennsylvania State University, 2010.
[48] M.P. Manahan, S. Kim, E.C. Kumbur, M.M. Mench, ECS Trans. 25 (2009) 1745–1754.
[49] Toyota Motor Company, Fickian diffusion coefficient ratio, Internal Communication to Penn State University, 2009.
[50] S. Kim, M. Khandelwal, C. Chacko, M.M. Mench, J. Electrochem. Soc. 156 (2009) B99–B108.
[51] S. Litster, D. Sinton, N. Djilali, J. Power Sources 154 (2006) 95–105.
[52] A. Turhan, K. Heller, J.S. Brenizer, M.M. Mench, J. Power Sources 180 (2008) 773–783.
[53] E.C. Kumbur, K.V. Sharp, M.M. Mench, J. Power Sources 176 (2008) 191–199.